View metadata, citation and similar papers at core.ac.uk

brought to you by CORE

provided by Open Archive Toulouse Archive Ouverte

Open Archive TOULOUSE Archive Ouverte (OATAO)

OATAO is an open access repository that collects the work of Toulouse researchers and makes it freely available over the web where possible.

This is an author-deposited version published in : http://oatao.univ-toulouse.fr/
Eprints ID : 6212

To link to this article : DOI: 10.1109/JSTARS.2012.2182760
URL : http://dx.doi.org/10.1109/JSTARS.2012.2182760

To cite this version : Shirvany, Reza and Chabert, Marie and Tourneret, Jean-Yves *Ship and Oil-Spill Detection Using the Degree of Polarization in Linear and Hybrid/Compact Dual-Pol SAR*. (2012) IEEE Journal of Selected Topics in Applied Earth Observations and Remote Sensing, vol. 5 (n° 3). pp. 885-892. ISSN 1939-1404

Any correspondence concerning this service should be sent to the repository administrator: staff-oatao@listes.diff.inp-toulouse.fr

Ship and Oil-Spill Detection Using the Degree of Polarization in Linear and Hybrid/Compact Dual-Pol SAR

Reza Shirvany, *Student Member, IEEE*, Marie Chabert, *Member, IEEE*, and Jean-Yves Tourneret, *Senior Member, IEEE*

***Abstract*—Monitoring and detection of ships and oil spills using synthetic aperture radar (SAR) have received a considerable attention over the past few years, notably due to the wide area coverage and day and night all-weather capabilities of SAR systems. Among different polarimetric SAR modes, dual-pol SAR data are widely used for monitoring large ocean and coastal areas. The degree of polarization (DoP) is a fundamental quantity characterizing a partially polarized electromagnetic field, with significantly less computational complexity, readily adaptable for on-board implementation, compared with other well-known polarimetric discriminators. The performance of the DoP is studied for joint ship and oil-spill detection under different polarizations in hybrid/compact and linear dual-pol SAR imagery. Experiments are performed on RADARSAT-2 C-band polarimetric data sets, over San Francisco Bay, and L-band NASA/JPL UAVSAR data, covering the Deepwater Horizon oil spill in the Gulf of Mexico.**

***Index Terms*—Compact polarimetry, deepwater horizon, degree of polarization (DoP), depolarization, dual-pol, hybrid, oil slick, oil spill, ship detection, synthetic aperture radar (SAR).**

I. Introduction

MARITIME surveillance is of great environmental and economical interest, directly contributing to improve public safety and environmental protection. In particular, efficiently monitoring the ships, oil platforms and oil spills are of critical importance. Oil spills are highly damaging to the environment and pose serious threats to ecology and wildlife in the marine system. Oil pollution comes partly from frequent illegal ship discharges and partly from large ship and oil-rig accidents, namely the Prestige tanker disaster (in 2002, northwest coast of Spain) and, more recently, the British Petroleum (BP) Deepwater Horizon oil spill (in 2010, northern Gulf of Mexico).

Maritime monitoring and surveillance using single- and linear dual-pol SAR modes have been extensively studied using RADARSAT-1, ERS-1/2, and ENVISAT ASAR data, demonstrating very promising results for ship detection and oil-spill identification (see, for example [1]–[6]). Maritime surveillance in SAR polarimetry can be made more reliable with the advent of new quad-pol (full polarimetric) SAR systems such as the Japanese ALOS-PALSAR, launched in January 2006, the Canadian RADARSAT-2, launched in December 2007, and the German TerraSAR-X, launched in June 2007. Moreover, the future launches of the European Sentinel-1 and the Canadian RADARSAT Constellation Mission (RCM), expected in 2014 with a notable interest in maritime surveillance, will mark a new era for the operational use of SAR data.

Full polarimetric systems alternately transmit two orthogonal polarizations and record both received polarizations, i.e., (HH, HV, VH, VV), where H and V denote the horizontal and vertical polarizations, respectively. In conventional dual-pol modes, only two linear polarizations are considered, i.e., (HH, HV), (VH, VV) and (HH, VV). Newly developed dual-pol SAR modes are hybrid and compact dual-pols, promoted in the literature for future SAR missions with the great advantage of providing a wider swath width, and hence greater area coverage compared to quad-pol systems. Souyris *et al.* [7] introduced the $\pi/4$ compact polarimetric (CP) mode, where the transmitted polarization is the superposition of linear horizontal and vertical polarizations and the received returns are recorded in both horizontal and vertical polarizations (45°H, 45°V). In a recent study, Raney [8] suggested a hybrid mode of operation, called CL-pol, with a right (or left) circular polarization on transmission and two linear polarizations on reception (RH, RV). The CL-pol mode is part of the design for the future RADARSAT constellation mission. Different dual-pol modes collect different aspects of the information content of the full polarimetric data, and thus, it is of great importance to study different dual-pol modes and select the appropriate configuration in each particular application.

In each dual-pol mode, the transmitted polarization characterizes the information extracted from a scene. The aim of this paper is to investigate the potential of a physically related polarimetric discriminator, the degree of polarization (DoP), for the detection of open water oil spills and man-made objects, e.g., buoys, ships, and oil/gas platforms, under different polarizations and incidence angles. The DoP has long been recognized as the most important parameter characterizing a partially polarized electromagnetic field [9], [10]. The DoP can help to determine the nature of the objects that backscatter the electromagnetic field. The DoP has not previously been applied to hybrid/compact dual-pol ship and oil spill detection. However, it may be of great interest for operational real-time detection thanks to its computationally efficient estimation.

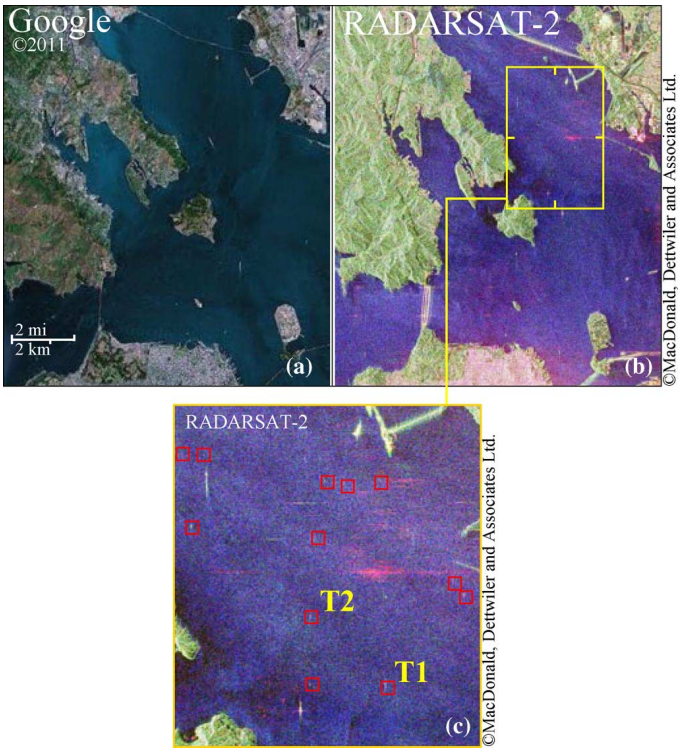

Fig. 1. San Francisco Bay, CA, USA. (a) Google Earth image of the area. (b) Pauli RGB image of the RADARSAT-2 fully polarimetric data set (Red, $|S_{\mathrm{HH}} - S_{\mathrm{VV}}|$; Green, $|S_{\mathrm{HV}} + S_{\mathrm{VH}}|$; Blue, $|S_{\mathrm{HH}} + S_{\mathrm{VV}}|$). (c) Zoom of the region of interest with 12 buoys (outlined by red boxes). T1 and T2 are two buoys studied in detail in Figs. 5 and 6. The original image has a size of 1816 × 3600 pixels.

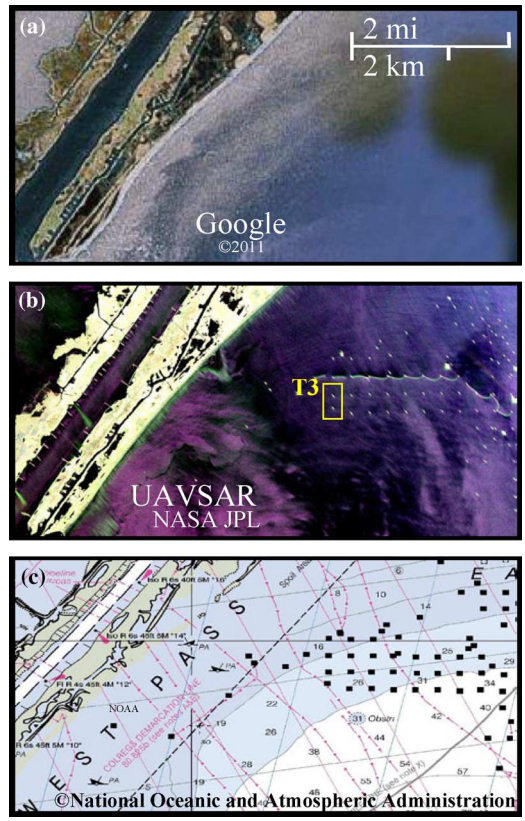

Fig. 2. Mississippi River Delta, LA, USA. (a) Google Earth image of the area. (b) Pauli RGB image of the NASA/JPL UAVSAR fully polarimetric data set (Red, $|S_{\mathrm{HH}} - S_{\mathrm{VV}}|$; Green, $|S_{\mathrm{HV}} + S_{\mathrm{VH}}|$; Blue, $|S_{\mathrm{HH}} + S_{\mathrm{VV}}|$). The box T3 outlines two oil-rigs studied in detail in Fig. 8. (c) NOAA nautical chart showing the position of the oil platforms (black boxes). The original image has a size of 1600 × 800 pixels.

We demonstrate the potentials of the DoP to enhance the contrast of man-made objects and oil spills against the surroundings when using different combinations of polarimetric SAR channels. We first analyze and compare the capabilities of DoP for different man-made object detection. Next, we study the oil-spill detection and slick type recognition in different dual-pol SAR data. In particular, we use L-band data acquired by NASA/JPL uninhabited aerial vehicle synthetic aperture radar (UAVSAR), over the northern Gulf of Mexico covering the Deepwater Horizon oil spill, and quad-pol data acquired by RADARSAT-2, over San Francisco Bay. Moreover, we compare the detection results in dual-pol modes with recent results, obtained using quad-pol data, presented by Marino *et al.* [11], [12]. This paper is organized as follows. In Section II, we review some physical and mathematical definitions and derive the estimator of the DoP in linear and hybrid/compact dual-pol modes. The data and study areas are presented in Section III. Experimental results and discussions for the detection of buoys, ships, oil rigs, and oil spills are presented in Section IV. Concluding remarks and future work are addressed in Section V.

II. Theory

The Jones vector [13] for an electromagnetic wave is defined by $\boldsymbol{E} = (E_1, E_2)^2$, where E_1 and E_2 are the orthogonal components of the electric field of the wave. In order to deal with a partially polarized wave, the Stokes parameters can be used. In 1852, Stokes [14] introduced four measurable quantities, known as the Stokes parameters, for describing the properties of polarized light. The Stokes parameters in linear polarization basis at the receiver, for a given incident polarization, are given by [15]

$$\begin{aligned} \mathrm{g}_1 &= |E_{\mathrm{H}}|^2 + |E_{\mathrm{V}}|^2 \\ \mathrm{g}_2 &= |E_{\mathrm{H}}|^2 - |E_{\mathrm{V}}|^2 \\ \mathrm{g}_3 &= 2\Re E_{\mathrm{H}} E_{\mathrm{V}}^* \\ \mathrm{g}_4 &= 2\Im E_{\mathrm{H}} E_{\mathrm{V}}^* \end{aligned} \tag{1}$$

where E is the complex electric field received in the subscripted polarization, i.e., horizontal or vertical (H or V), * denotes complex conjugate, and $\Re$ and $\Im$ denote the real and imaginary parts of the complex field, respectively. Note that the transmit polarization is not included in the subscripts. The transmit polarization for a traditional dual-pol radar is either H or V, for the CL-pol mode is either left- or right-circular (L and R), and for the $\pi/4$ compact mode is H + V oriented at 45°.

The electric vector $\boldsymbol{E}^{\mathrm{r}}$ of the received (or backscattered) field and the transmitted (or incident) field $\boldsymbol{E}^{\mathrm{t}}$ are related by

$$\boldsymbol{E}^{\mathrm{r}} = \boldsymbol{S}\boldsymbol{E}^{\mathrm{t}} \quad \boldsymbol{S} = \begin{pmatrix} S_{\mathrm{HH}} & S_{\mathrm{HV}} \\ S_{\mathrm{VH}} & S_{\mathrm{VV}} \end{pmatrix} \tag{2}$$

where $\boldsymbol{S}$ is the scattering matrix, known as the Sinclair matrix [16]. In the bistatic scattering case, the quad-pol scattering

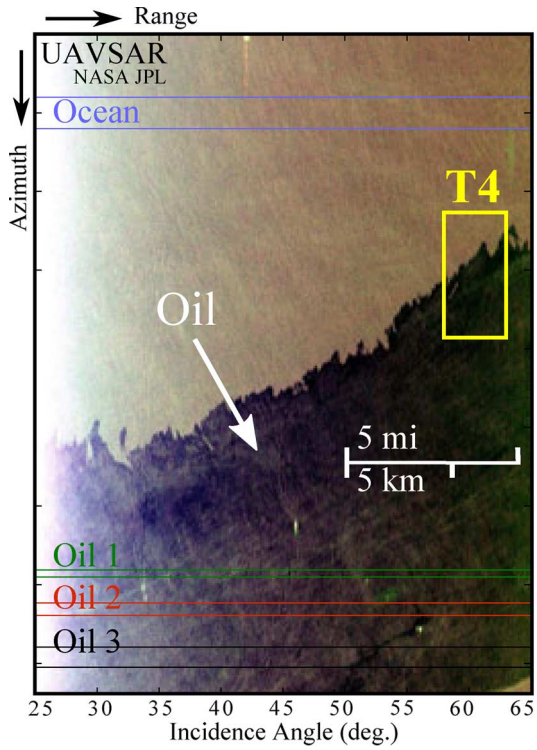

Fig. 3. Pauli RGB image of the NASA/JPL UAVSAR fully polarimetric data set from the Deepwater Horizon oil spill in northern Gulf of Mexico, USA. (Red, $|S_{\rm HH} - S_{\rm VV}|$; Green, $|S_{\rm HV} + S_{\rm VH}|$; Blue, $|S_{\rm HH} + S_{\rm VV}|$). The oil appears as a dark patch within the ocean clutter. The outlined regions of oil (oil 1–3) and ocean are used in Fig. 9 to study the oil spill detection. The box T4 outlines a region of interest further studied in Fig. 10. The original image has a size of 3151 × 4201 pixels.

vector corresponding to the Sinclair matrix is defined as $\vec{k}_{\rm FP} = (S_{\rm HH}, S_{\rm HV}, S_{\rm VH}, S_{\rm VV})^T$ [17]. The dual-pol scattering vectors in (HH, HV), (VH, VV), and (HH, VV) modes are, respectively, defined by

$$\begin{aligned}\vec{k}_{\rm DP1} &= (S_{\rm HH}, S_{\rm HV})^T \\ \vec{k}_{\rm DP2} &= (S_{\rm VH}, S_{\rm VV})^T \\ \vec{k}_{\rm DP3} &= (S_{\rm HH}, S_{\rm VV})^T. \end{aligned} \tag{3}$$

Hybrid/compact dual-pol scattering vectors can be simulated from quad-pol data using (2). In CL-pol mode, for example, a right-circular illumination is obtained by $\boldsymbol{E}^t = 1/\sqrt{2}(1, -j)^T$, and thus $\boldsymbol{E}^r = 1/\sqrt{2}(S_{\rm HH} - iS_{\rm HV}, -iS_{\rm VV} + S_{\rm VH})^T$. Hence, the corresponding scattering vector is defined by $\vec{k}_{\rm CL-pol} = (E_{\rm H}, E_{\rm V})^T$ where $E_{\rm H} = (1, 0)\boldsymbol{E}^r$ and $E_{\rm V} = (0, 1)\boldsymbol{E}^r$. The scattering vector for the $\pi/4$ mode can be derived in the same fashion. Hence, hybrid/compact dual-pol scattering vectors can be written as

$$\begin{aligned}\vec{k}_{\pi/4} &= \frac{1}{\sqrt{2}}(S_{\rm HH} + S_{\rm HV}, S_{\rm VV} + S_{\rm VH})^T \\ \vec{k}_{\rm CL-pol} &= \frac{1}{\sqrt{2}}(S_{\rm HH} - iS_{\rm HV}, -iS_{\rm VV} + S_{\rm VH})^T. \end{aligned} \tag{4}$$

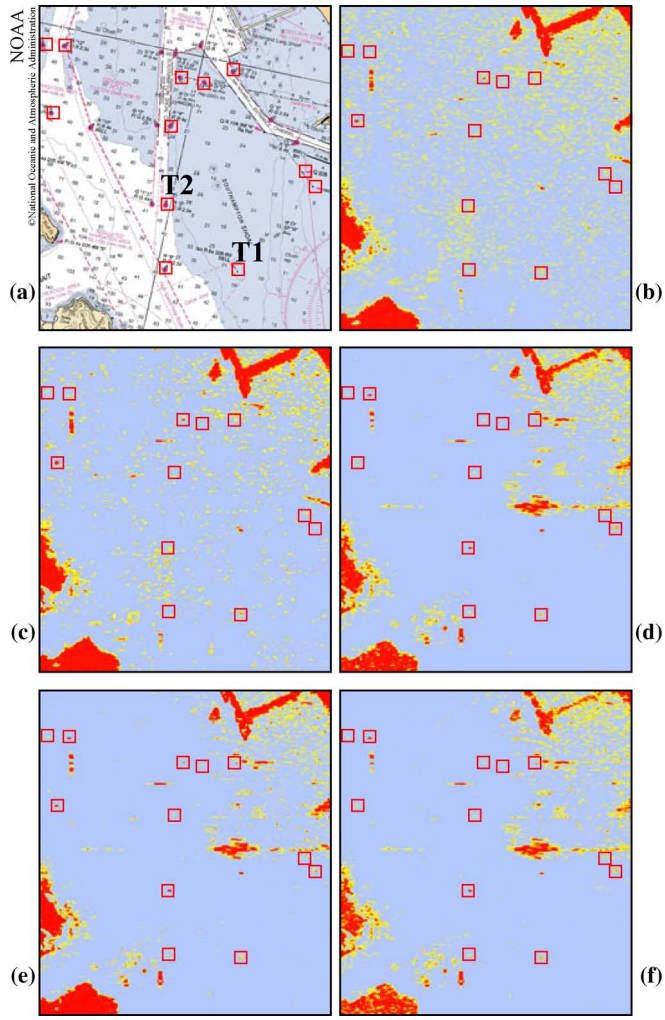

Fig. 4. (a) NOAA nautical chart showing the position of the buoys. (b)–(f) Maps of the degree of polarization over the San Francisco Bay test area (outlined in Fig. 1) in different hybrid/compact and linear dual-pol modes. (b) HH-HV. (c) VH-VV. (d) HH-VV. (e) CL-pol. (f) $\pi/4$.

We note that, under the scattering reciprocity, and in the backscatter alignment convention, we have $S_{\rm HV} = S_{\rm VH}$ [18].

The state of polarization of an electromagnetic wave can be characterized by the DoP expressed, in terms of the Stokes parameters, as

$$\mathcal{P} = \frac{\sqrt{\rm g_2^2 + g_3^2 + g_4^2}}{\rm g_1}. \tag{5}$$

Mathematically, on the Poincaré sphere, the DoP represents the distance of a normalized Stokes vector's last three components from the origin. The surface of the unit Poincaré sphere corresponds to $\mathcal{P} = 1$ and represents all totally polarized states [19]. Depolarization is associated with a reduction in the DoP of incident states.

The degree of depolarization (DoD) is defined as $\overline{\mathcal{P}} = 1 - \mathcal{P}$. A depolarizing interaction causes totally polarized Stokes states on the surface of the Poincaré sphere to emerge with $\mathcal{P} < 1$, and thus $\overline{\mathcal{P}} > 0$. In brief, the wave is totally depolarized for $\overline{\mathcal{P}} = 1$ ($\mathcal{P} = 0$), totally polarized for $\overline{\mathcal{P}} = 0$ ($\mathcal{P} = 1$), and partially polarized when $\overline{\mathcal{P}}, \mathcal{P} \in]0, 1[$. The DoP, and thus the DoD, are invariant with respect to the choice of orthogonal polarization

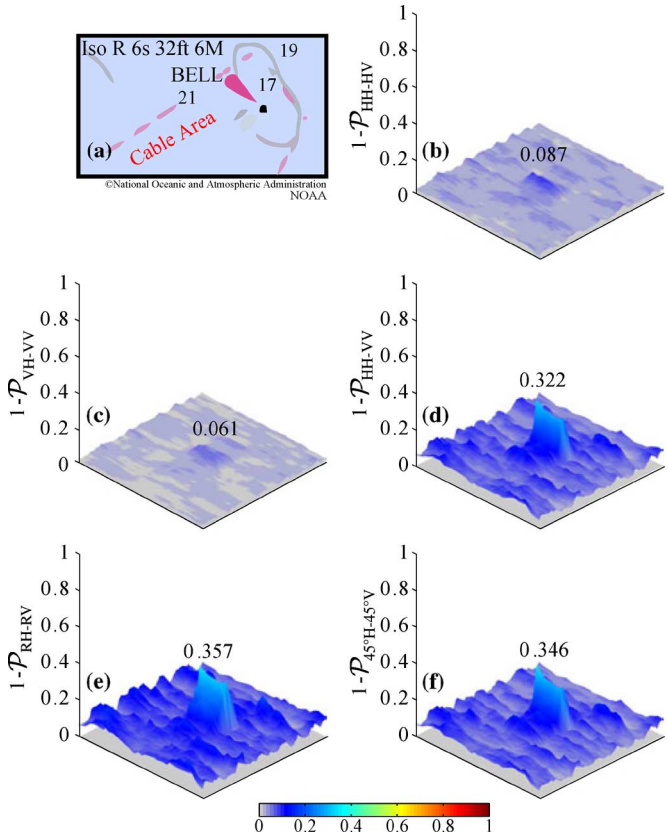

Fig. 5. San Francisco Bay, CA, USA. (a) NOAA nautical chart showing the position of Southampton Shoal day mark (T1). (b)–(f) Degree of depolarization in different hybrid/compact and linear dual-pol modes. (b) HH-HV. (c) VH-VV. (d) HH-VV. (e) CL-pol. (f) $\pi/4$.

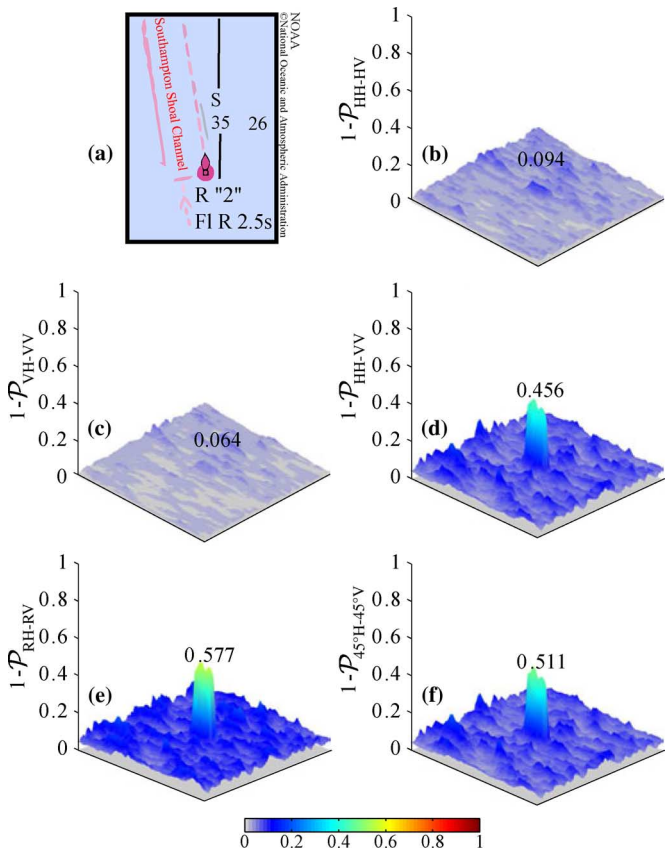

Fig. 6. San Francisco Bay, CA, USA. (a) NOAA nautical chart showing the position of Southampton Shoal Channel Entrance buoy (T2). (b)–(f) Degree of depolarization in different hybrid/compact and linear dual-pol modes. (b) HH-HV. (c) VH-VV. (d) HH-VV. (e) CL-pol. (f) $\pi/4$.

basis at the receiver. However, DoD and DoP are dependent of the transmit polarization. Hence, the nature of the application and targets of interest determine the optimal transmit polarization. The DoP and DoD are estimated in each dual-pol mode by

$$\mathcal{P} = \frac{\sqrt{\widehat{\alpha}_2^2 + \widehat{\alpha}_3^2 + \widehat{\alpha}_4^2}}{\widehat{\alpha}_1}, \quad \overline{\mathcal{P}} = 1 - \mathcal{P} \tag{6}$$

with $\widehat{\alpha}_l = (1/n)\sum_{j=1}^{n} \mathrm{g}_l[j], l = 1, \ldots, 4$, where n is the number of samples used for the estimation, and $\mathrm{g}_l[j]$ is the lth Stokes parameter associated with the jth pixel. In other words, $\widehat{\alpha}_l$ is calculated for each pixel by using a sliding square window centered on the considered pixel and computing the empirical mean over the n pixels contained in the window. We note that the estimation of the DoP involves significantly low computational complexity and is readily adaptable for on-board implementation. In this study, the sensitivity of the DoP with respect to different polarizations is investigated for the discrimination of man-made objects and oil spills from the sea surface. We estimate the DoP in hybrid/compact and linear dual-pol SAR modes and compare the detection performance of these modes for different scenarios.

III. Data and Study Sites

In the present paper, we use C-band data acquired by RADARSAT-2, as well as L-band data acquired by NASA/JPL UAVSAR. RADARSAT-2 is a Canadian C-band SAR satellite launched in December 2007. It provides many operating modes, including linear dual- and quad-pol modes, and supports right- and left-look imaging. The NASA/JPL UAVSAR, operational since 2007, is a reconfigurable fully polarimetric L-band (1.26 GHz, 24-cm wavelength) airborne system with a range bandwidth of 80 MHz (2-m range resolution) and a range swath greater than 16 km.

The RADARSAT-2 data set is acquired in fine quad-pol mode over San Francisco Bay, California (37°45′0″N, 122°17′0″W). The Google Earth and Pauli RGB images of this data set are shown in Fig. 1. RADARSAT-2 data are used for detection of ships, boats, and buoys. Furthermore, oil/gas platform detection is studied using NASA/JPL UAVSAR data sets over northern Gulf of Mexico, Mississippi River Delta, Louisiana (29°0′43.56″N, 89°15′33.12″W). The Google Earth and Pauli RGB images of this data set are shown in Fig. 2. We analyze the depolarization signatures of oil spills, under different incidence angles and polarizations, using the Deepwater Horizon oil spill data (28°44′11.86″N, 88°21′57.59″W), acquired in quad-pol mode by NASA/JPL UAVSAR on June 22–23, 2010. The Deepwater Horizon oil spill occurred on April 20, 2010, in the Gulf of Mexico, is by far the worst oil spill in U.S. history, with over 200 million gallons of leaked oil. The Pauli RGB image of the oil spill study region is shown in Fig. 3.

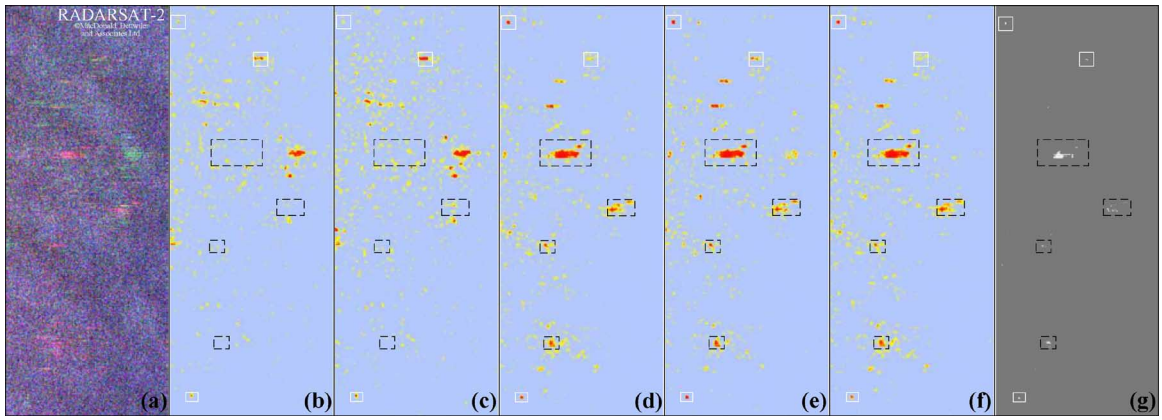

Fig. 7. (a) Pauli RGB image of a test area from San Francisco Bay, RADARSAT-2 fully polarimetric data set. (b)–(f) Maps of the degree of polarization over the test area in different hybrid/compact and linear dual-pol modes. (b) HH-HV. (c) VH-VV. (d) HH-VV. (e) CL-pol. (f) $\pi/4$. (g) Ship-detection results, based on quad-pol data, reported by Marino *et al.* [11], [12]. Boxes indicate potential ships; solid (white) boxes indicate targets that are visible in all modes whereas dashed (black) boxes indicate less visible or non visible targets in linear dual-pol modes.

IV. Experimental Results and Discussion

A. Buoy Detection

Buoys are distinctively shaped floating devices with many different purposes. In this section, we consider the buoy detection task whose performance can be evaluated accurately thanks to the precise nautical charts reporting the exact position of the buoys via different systems. For this purpose, we use nautical charts from National Oceanic and Atmospheric Administration (NOAA) as ground truths. Fig. 4(a) shows an NOAA nautical chart over a test region in San Francisco Bay with 12 buoys of interest (red boxes). The maps of the DoP obtained over this region, for linear and hybrid/compact dual-pol modes, are shown in Fig. 4(b)–(f). Thresholds were manually chosen so that a maximum number of targets is visible. We note that most of the buoys which can hardly be seen in linear dual-pol modes [Fig. 4(b) and (c)], are easily distinguished in hybrid/compact modes [Fig. 4(e) and (f)]. The latter is further demonstrated in Figs. 5 and 6. These figures show the DoD surfaces for Southampton Shoal day mark [height = 32 ft/9.75 m, marked as T1 in Fig. 4(a)], and Southampton Shoal Channel Entrance buoy (T2). We see the gain of performance for buoy detection when using hybrid/compact dual-pol data compared to linear (HH, HV) and (VH, VV) data. We note that the results from (HH, VV) mode [Fig. 4(d)] are closely comparable to hybrid/compact modes.

B. Ship Detection

Here, we study the performance of the DoP in a ship-detection context. For this purpose, we compare the DoP maps of San Francisco Bay region to the results recently reported by Marino *et al.* [11], [12]. Fig. 7(a) shows the Pauli RGB images of a region of interest from RADARSAT-2 San Francisco Bay data set. Fig. 7(b)–(f) shows the maps of the DoP obtained in hybrid/compact and linear dual-pol modes over the test region (thresholds were manually chosen so that a maximum number of targets is visible). Fig. 7(g) shows the ship-detection results reported by Marino *et al.* [11], [12] obtained using a notch filter based on quad-pol SAR data. In these figures, boxes indicate potential ships; solid (white) boxes indicate targets that are visible in all modes whereas dashed (black) boxes indicate less visible or nonvisible targets in linear dual-pol modes. We see that most of the ships detected using the quad-pol method [Fig. 7(g)] are not visible in the (HH, HV) and (VH, VV) dual-pol modes (black, dashed boxes) whereas they are clearly seen in (HH, VV) and hybrid/compact dual-pol modes.

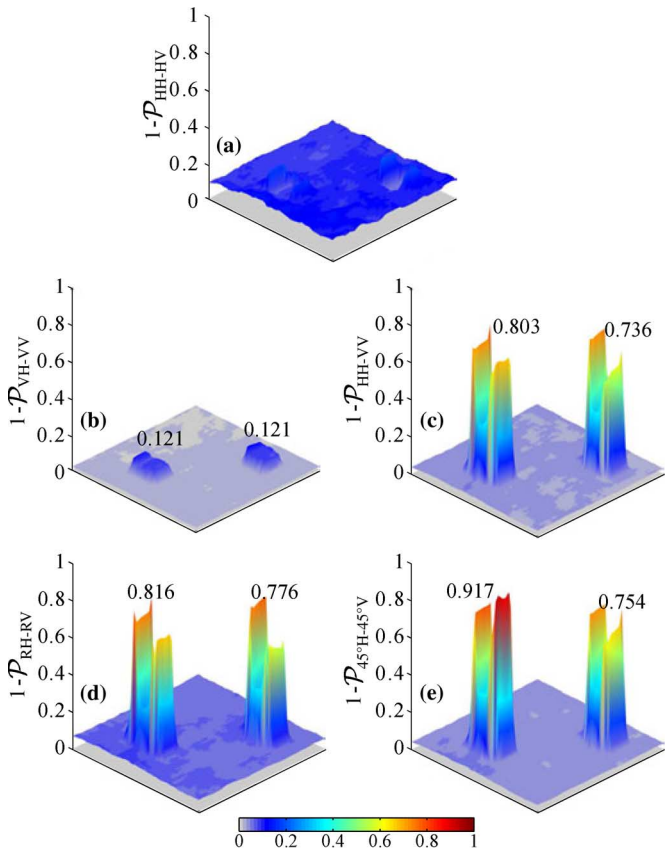

Fig. 8. Degree of depolarization for oil platforms (T3) in the Mississippi River Delta, LA, USA. (a) HH-HV. (b) VH-VV. (c) HH-VV. (d) CL-pol. (e) $\pi/4$.

It is important to emphasize that the ship-detection results based on the estimation of the DoP in hybrid/compact dual-pol

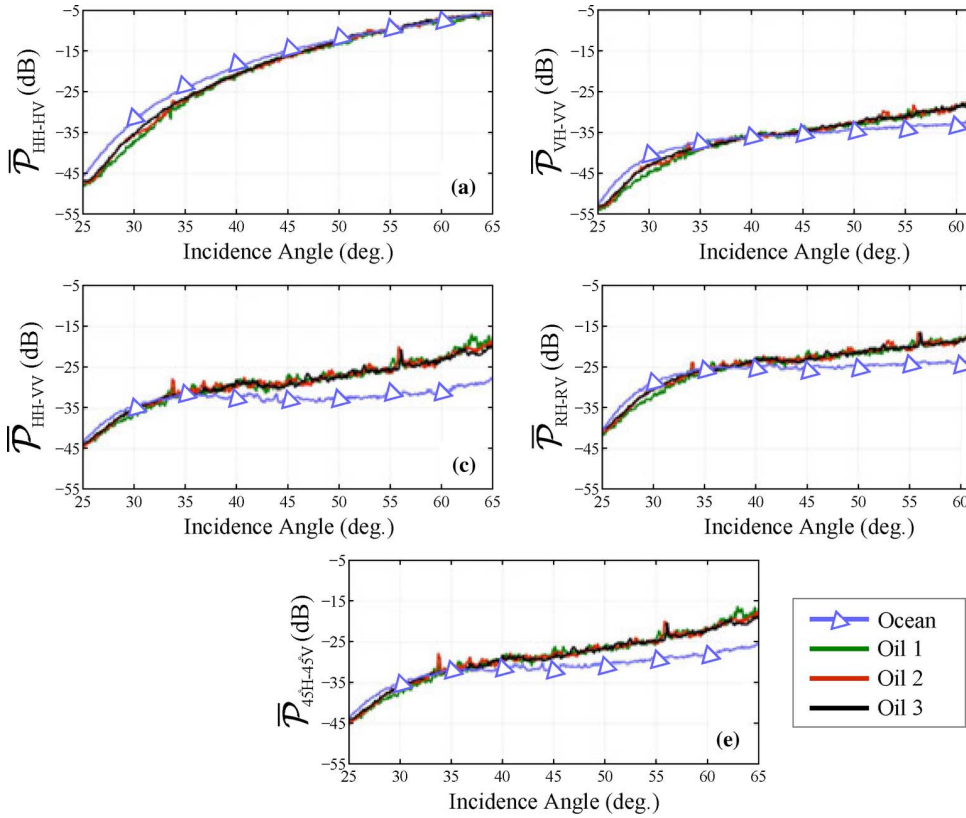

Fig. 9. Depolarization $\overline{\mathcal{P}}$ (dB) versus incidence angle (deg.) for ocean and oil regions in different hybrid/compact and linear dual-pol modes. (a) HH-HV. (b) VH-VV. (c) HH-VV. (d) CL-pol. (e) $\pi/4$. Regions are shown in Fig. 3.

modes are closely comparable to the notch filter results which are obtained using quad-pol data, enjoying the full polarimetric information of the scene. These results are in agreement with those obtained in the buoy detection case. However, we highlight that the ship-detection problem is slightly different from the previous buoy detection context; in particular, ships are much bigger than buoys, and thus they can introduce a preferred direction. Therefore, some ships, because of their alignment, may be more visible in some dual-pol modes than the others.

C. Oil-Rig Detection

Wide-area identification of oil and gas platforms after hurricanes and storms is of critical importance. It allows the reconnaissance flights to be carried out much more efficiently, resulting in significant savings and increased safety. In the context of oil-rig detection, Gulf of Mexico with nearly 4000 active oil and gas platforms is an interesting study case. Fig. 2 shows the Google Earth and Pauli RGB images of a test region in northern Gulf of Mexico, along with a NOAA nautical chart reporting the position of oil and gas platforms. Most of the targets are bright enough to be visible on the Pauli RGB image. The DoD surfaces showing two oil platforms (marked as T3 in Fig. 2) are shown in Fig. 8. Once again, we notice that hybrid/compact and (HH, VV) modes clearly detect the oil-rigs whereas (HH, HV) and (VH, VV) modes are less performant. We note that DoP signatures are representative of different scattering mechanisms in a scene. Hence, the DoP surfaces can also help in target identification (for example distinguishing between buoys, ships, and oil rigs). This is an interesting subject for future work.

D. Oil Spill Detection and Identification

Oil spreads as thin layers on the surface of the ocean. The influence of surface oil on ocean backscatter has been extensively studied using single-pol radar data (see, for example, [4]–[6]). Oil spills have a different constitution than water; they dampen the small-scale ocean surface waves, Bragg waves [20], and cause weaker radar backscatter signatures. As a result, oil regions on the SAR images appear as dark patches within ocean clutter (see Fig. 3). There exists a limited number of studies on the use of polarimetric discriminators for enhancing oil spill detection. In particular, the utility of entropy, anisotropy, and average alpha of the Cloude–Pottier decomposition [21] has been recently investigated for oil-spill detection [22]–[24]. Other decompositions, such as Shannon entropy decomposition [25], have also been newly studied by NASA/JPL for oil spill characterization [26]. However, such parameters can only be calculated using full polarimetric SAR data.

We study in what follows the depolarization signatures of oil spills and clear water in different dual-pol SAR modes. We use homogeneous regions of oil and water, covering all the incidence angle range, i.e., from 25° to 65° (near- to far-range), as shown in Fig. 3. The depolarization profile of these regions are shown in Fig. 9. All dual-pol modes discriminate water and oil for most of the incidence angle range. These results show that, in shallow incidence angles, (HH, VV) mode outperforms other

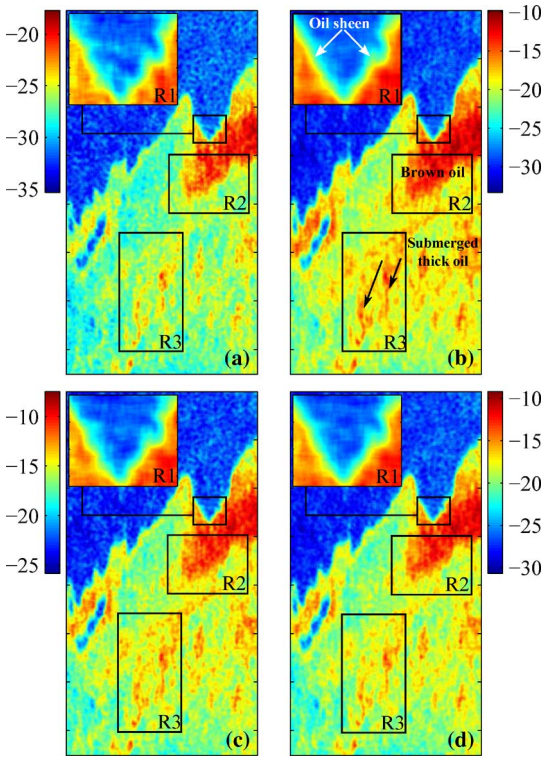

Fig. 10. Oil-slick property/type recognition using the degree of depolarization $\overline{\mathcal{P}}$ (dB) in dual-pol SAR. (a) VH-VV. (b) HH-VV. (c) CL-pol. (d) $\pi/4$. The region is a subset of UAVSAR data set outlined as T4 in Fig. 3.

modes whereas in steeper incident angles, (HH, HV) outperforms other modes in distinguishing oil from water. The detection results from hybrid/compact dual-pol modes (CL-pol and $\pi/4$) are close to (HH, VV). We notice that the clear water depolarizes the incident wave more than oil for steep incidence angles, and less than oil for shallow incidence angles. The transition incidence angle is around 40°.

Identifying the color, structure, and consistency of oil on water can help to determine the oil type, the amount of time it has been on the water, and other information, critical to improve the oil-recovery process. The thinnest possible oil layer is called sheen, which dampens out the surface waves and gives the water a reflective appearance. Thicker oil layers are called rainbow, metallic, transitional, and dark oil slick. Depolarization maps of oil spills are further studied in Fig. 10 for oil-property recognition in different dual-pol SAR modes. In each figure, three regions of interest (R1, R2, and R3) are outlined. All depolarization maps reveal the oil structures and properties in different dual-pol modes with (HH, VV) giving the maximum depolarization contrast between dark oil and clear water. Using these depolarization maps, we can recognize the oil sheens along the edges (in R1 region), the dark oil patches (in R2 region), and also the narrow bands of oil (in R3 region) revealing the direction of the wind.

V. Conclusion

The DoP was used to detect the features, such as man-made objects and oil spills, with different polarimetric signatures compared with the sea clutter. The detection performance of the degree of polarization was studied in different hybrid/compact and linear dual-pol SAR modes. It was shown that the DoP provides valuable information for man-made object and oil-spill detection under different polarizations and incidence angles. Experiments were performed on RADARSAT-2 C-band polarimetric data sets, over San Francisco Bay, and L-band NASA/JPL UAVSAR data, covering the Deepwater Horizon oil spill in the Gulf of Mexico. Experimental results suggest that hybrid/compact and (HH, VV) dual-pol modes deliver better detection performance compared to conventional dual-pol modes, i.e., (HH, HV) and (VH, VV). Investigated polarization signatures are of interest in joint detection of ships and oil spills, using dual-pol SAR data, in large coastal and ocean areas under all-weather conditions.

Acknowledgment

The authors would like to thank R. Touzi and A. Marino for fruitful discussions and suggestions at IGARSS'11. The authors would also like to acknowledge NASA Jet Propulsion Laboratory (JPL) and Alaska Satellite Facility (ASF) for providing UAVSAR data, and MacDonald, Dettwiler and Associates Ltd. (MDA), for making available the RADARSAT-2 data used in this paper.

References

[1] P. W. Vachon, J. W. M. Campbell, C. Bjerkelund, F. W. Dobson, and M. T. Rey, "Ship detection by the RADARSAT SAR: Validation of detection model predictions," *Can. J. Remote Sens.*, vol. 23, no. 1, pp. 48–59, 1997.

[2] R. Touzi, F. J. Charbonneau, R. K. Hawkins, and P. W. Vachon, "Ship detection and characterization using polarimetric SAR," *Can. J. Remote Sens.* vol. 30, no. 3, pp. 552–559, 2004.

[3] C. Liu, P. W. Vachon, and G. W. Geling, "Improved ship detection using polarimetric SAR data," in *Proc. IGARSS*, Anchorage, AK, Sep. 2004, vol. 3, pp. 1800–1803, vol. 3.

[4] K. Singh, A. Gray, R. Hawkins, and R. O'Neil, "The influence of surface oil on C-and Ku-band ocean backscatter," *IEEE Trans. Geosci. Remote Sens.*, vol. GE-24, no. 5, pp. 738–744, Sep. 1986.

[5] V. Wismann, M. Gade, W. Alpers, and H. Hühnerfuss, "Radar signatures of mineral oil spills measured by an airborne multi-frequency multi-polarization microwave scatterometer," in *Proc. OCEANS Eng. Harmony With Ocean*, Victoria, BC, Canada, Oct. 1993, vol. 2, pp. II348–II353.

[6] M. F. Fingas and C. E. Brown, "Review of oil spill remote sensing," *Spill Sci. Technol. Bull.* vol. 4, no. 4, pp. 199–208, 1997.

[7] J.-C. Souyris, P. Imbo, R. Fjortoft, S. Mingot, and J.-S. Lee, "Compact polarimetry based on symmetry properties of geophysical media: The $\pi/4$ mode," *IEEE Trans. Geosci. Remote Sens.*, vol. 43, no. 3, pp. 634–646, Mar. 2005.

[8] R. Raney, "Hybrid-polarity SAR architecture," *IEEE Trans. Geosci. Remote Sens.*, vol. 45, no. 11, pp. 3397–3404, Nov. 2007.

[9] R. C. Jones, "A new calculus for the treatment of optical systems: A more general formulation and description of another calculus," *J. Opt. Soc. Amer.* vol. 37, no. 2, pp. 107–110, 1947.

[10] E. Wolf, "Coherence properties of partially polarized electromagnetic radiation," *Nuovo Cim.*, vol. 13, no. 6, pp. 1165–1181, Sep. 1959.

[11] A. Marino, N. Walker, and I. Woodhouse, "Ship detection using SAR polarimetry. The development of a new algorithm designed to exploit new satellite SAR capabilities for maritime surveillance," in *Proc. SeaSAR*, Rome, Italy, Jan. 2010.

[12] A. Marino, N. Walker, and I. Woodhouse, "Ship detection with RADARSAT-2 quad-pol SAR data using a notch filter based on perturbation analysis," in *Proc. IGARSS*, Honolulu, HI, Jul. 2010, pp. 3704–3707.

[13] R. C. Jones, "A new calculus for the treatment of optical systems," *J. Opt. Soc. Amer.* vol. 31, no. 7, pp. 488–493, Jul. 1941.

[14] G. G. Stokes, "On the composition and resolution ofstreams of polarized light from different sources," *Trans.Camb. Philosoph. Soc.*, vol. 9, pp. 399–416, Jul. 1852.

[15] P. E. Green, Jr., "Radar measurements of target scattering properties," in *Radar Astronomy*, J. V. Evans and T. Hagfors, Eds. New York: McGraw-Hill, 1968, pp. 1–78.
[16] A. Guissard, "Mueller and Kennaugh matrices in radar polarimetry," *IEEE Trans. Geosci. Remote Sens.*, vol. 32, no. 3, pp. 590–597, May 1994.
[17] J.-S. Lee and E. Pottier, *Polarimetric Radar Imaging: From Basics to Applications*. Boca Raton, FL: CRC, 2009.
[18] S. V. Nghiem, S. H. Yueh, R. Kwok, and F. K. Li, "Symmetry properties in polarimetric remote sensing," *Radio Sci.*, vol. 27, pp. 693–711, Oct. 1992.
[19] C. Brosseau, *Fundamentals of Polarized Light: A StatisticalOptics Approach*. New York: Wiley, 1998.
[20] G. R. Valenzuela, "Theories for the interaction ofelectromagnetic and oceanic waves a review," *Boundary-Layer Meteorol.* vol. 13, pp. 61–85, 1978.
[21] S. Cloude and E. Pottier, "A review of target decomposition theorems in radar polarimetry," *IEEE Trans. Geosci. Remote Sens.*, vol. 34, no. 2, pp. 498–518, Mar. 1996.
[22] J. Fortuny-Guasch, "Improved oil slick detection andclassification with polarimetric SAR," in *Proc. POLin-SAR*, Frascati, Italy, Jan. 14–16, 2003, p. 27.1.
[23] D. Schuler, J. Lee, and G. De Grandi, "Spiral eddy detection using surfactant slick patterns and polarimetric SAR image decomposition techniques," in *Proc. IGARSS*, Anchorage, AK, Sep. 2004, vol. 1, pp. 212–215.
[24] M. Migliaccio, A. Gambardella, and M. Tranfaglia, "SAR polarimetry to observe oil spills," *IEEE Trans. Geosci. Remote Sens.*, vol. 45, no. 2, pp. 506–511, Feb. 2007.
[25] P. Réfrégier and J. Morio, "Shannon entropy of partially polarized and partially coherent light with Gaussian fluctuations," *J. Opt. Soc. Amer. A* vol. 23, no. 12, pp. 3036–3044, Dec. 2006.
[26] C. Jones, B. Minchew, and B. Holt, "Polarimetric decomposition analysis of the Deepwater Horizon oil slick using L-band UAVSAR data," in *Proc. IGARSS*, Vancouver, BC, Canada, Jul. 2011, pp. 2278–2281.

Reza Shirvany (S'06) received the M.E. degree (diplôme d'ingénieur) in electrical engineering from École Nationale Supérieure d'Électronique, d'Électrotechnique, d'Informatique, d'Hydraulique, et des Télécommunications (ENSEEIHT), Toulouse, France, and the M.Sc. degree in signal and image processing from Institut National Polytechnique de Toulouse (INPT), Toulouse, France, both in 2008. He is currently working toward the Ph.D. degree at the University of Toulouse, Toulouse, France,

He was a Research Intern with the Biomedical Imaging Group, École Polytechnique Fédérale de Lausanne (EPFL), Lausanne, Switzerland, working on B-splines and wavelets. His main research interest lies in mathematical modelling and applications of polarimetric imagery.

Marie Chabert (M'10) received the Eng. degree in electronics and signal processing from ENSEEIHT, Toulouse, France, in 1994, and the M.Sc. degree in signal processing, Ph.D. degree in signal processing, and Habilitation aά Diriger les Recherches (HDR) from the National Polytechnic Institute of Toulouse, Toulouse, France, in 1994, 1997, and 2007, respectively.

She is an Associate Professor of signal and image processing with INPT-ENSEEIHT, University of Toulouse. She is conducting her research with the Signal and Communication team of the Institute de Recherche en Informatique de Toulouse IRIT (UMR 5505 of the CNRS). Her research interests include nonuniform sampling, time–frequency diagnosis and condition monitoring, and statistical modeling of heterogenous data in remote sensing.

Jean-Yves Tourneret (SM'08) received the ingénieur degree in electrical engineering from the École Nationale Supérieure d'Électronique, d'Électrotechnique, d'Informatique, d'Hydraulique, et des Télécommunications (ENSEEIHT), Toulouse, France, in 1989, and the Ph.D. degree from the National Polytechnic Institute, Toulouse, in 1992.

He is currently a Professor with the University of Toulouse (ENSEEIHT) and a member of the IRIT laboratory (UMR 5505 of the CNRS). His research activities are centered around statistical signal processing with a particular interest to Bayesian methods and Markov chain Monte Carlo (MCMC) algorithms.